The European Journal of Research and Development

journals.orclever.com/ejrnd

OR CLEVER Science & Research Group

Research Article

An Evaluation of Radiation Performances of Various Aperture and Horn Antennas over Sea Surface

Doaa Salim Mohammed Musa, Ramazan Daşbaşı*, Burak Polat,

Yildiz Technical University, Department of Electronics and Communications Engineering, Istanbul, Turkey, https://orcid.org/0000-0002-5668-8946, doaa.mohammed.musa@std.yildiz.edu.tr; https://orcid.org/0000-0002-7706-2053, rdasbasi@yildiz.edu.tr; https://orcid.org/0000-0002-3188-2670, abpolat@yildiz.edu.tr.

* Correspondence: rdasbasi@yildiz.edu.tr

(First received March 05, 2022 and in final form May 22, 2022)

Reference: Musa, D. S. M., Daşbaşı, R., & Polat, B. An Evaluation of Radiation Performances of Various Aperture and Horn Antennas over Sea Surface. *The European Journal of Research and Development*, 2(2), 429–444.

Abstract

Directional Currents Method (DCM) is applied to various aperture and horn antennas including rectangular aperture antenna, circular aperture antenna, dielectric loaded rectangular aperture antenna and E- and H-plane sectoral horn antennas to investigate their radiation performances analytically over sea surface in microwave bands. First, the expressions of the hypothetical directional currents of these antennas are derived in free space and the total radiation patterns are generated by MATLAB™. Then, the same antennas are simulated by the commercial electromagnetic simulation software CST™ and compared to check the parametric accuracy of DCM numerically. In the second step, these directional currents are employed in deriving the analytical radiation fields of the antennas under investigation over sea surface by incorporating Green's functions based on Norton's formulation. This is followed by CST™ simulations to observe the parametric accuracy of DCM expressions for microwave radiation over sea surface.

Keywords: Aperture antenna, horn antenna, radiation over ground, surface waves.

1. Introduction

Antennas are structures that are used for transferring the power carried through cables or waveguides to transmission media and vice versa. These devices are one of the most essential parts of modern wireless communication networks, radar and satellite

systems, etc. There exist many types of antennas such as wire antennas, aperture antennas, horn antennas, reflector antennas, microstrip patch antennas, and so on.

The attention in the present work is focused on aperture and horn antennas, which are broadly in microwave communication/radar systems as primary or feed antennas. They are also enrolled as reference antennas in gain and radiation pattern measurements. The simplicity of their mechanical structure is suitable for rapid manufacturing, even with 3-D printer technology.

The analytical radiation fields of these types of antennas in free space are studied for many decades and are available in reference antenna textbooks (cf.[1],[2]). However, the analytical radiation fields of these antennas over a lossy dielectric half-space are not broadly investigated in literature. To fill this gap the Directional Currents Method (DCM) has been developed by Polat & Daşbaşı in 2020 [3] with applications to pyramidal horn antennas over a lossy dielectric half-space under High Contrast Approximation (HCA). In 2021 the method has been extended to cover conical [4] and corrugated conical [5] horn antennas for the same scenario.

In this method, free space radiation fields of aperture and horn antennas - which are already available in the literature based on surface equivalence theorems - are matched with the radiation fields of a cross-polarized vertical electric dipole (VED) and a horizontal magnetic dipole (HMD) over the aperture surface. Once the hypothetical directional current distributions on the dipoles are obtained, we insert these currents into Norton's formulations [6], [7] (derived under HCA acting on the refractivity of the interface) for the far fields of ideal VED and HMD sources with unit dipole moments and apply Principle of Superposition to derive the total radiation fields.

In Section 2 we derive the expressions of the hypothetical directional currents of the antennas under investigation in free space and the total radiation patterns are generated by MATLAB™. Then, the same antennas are simulated by the commercial electromagnetic simulation software CST™ and compared to check the parametric accuracy of DCM numerically.

In Section 3 these directional currents are employed in deriving the analytical radiation fields of the antennas under investigation over sea surface by incorporating Green's functions based on Norton's formulation. This is followed by CST™ simulations to observe the parametric accuracy of DCM expressions for microwave radiation over sea surface.

Through the paper time dependence $\exp(-i\omega t)$, where ω is the angular frequency of radiation, is assumed and suppressed.

2. Directional Currents for Aperture and Horn Antennas

Directional currents are hypothetical currents that flow through cross-polarized VED and HMD sources located on the aperture surface of the interested antenna such that their total radiation fields

$$E_\theta(\theta,\phi)=\frac{i\omega}{4\pi}\left[\mu I_e(\theta,\phi)\cos\theta-\varepsilon\eta I_m(\theta,\phi)\right]\sin\phi \tag{1}$$

$$E_\phi(\theta,\phi)=\frac{i\omega}{4\pi}\left[\mu I_e(\theta,\phi)-\varepsilon\eta I_m(\theta,\phi)\cos\theta\right]\cos\phi \tag{2}$$

in spherical coordinates match with that of the physical antenna. In (1) and (2) $I_e(\theta,\phi)$ and $I_m(\theta,\phi)$ are electric and magnetic directional currents flowing on VED and HMD, respectively where (ε,μ) are the constitutive parameters and $\eta=\sqrt{\mu/\varepsilon}$ is the characteristic impedance of the radiation medium.

2.1. Rectangular Aperture Mounted on an Infinite Ground Plane

A rectangular aperture antenna (RAA) with dimensions a and b on an infinite ground is illustrated in Figure 1.

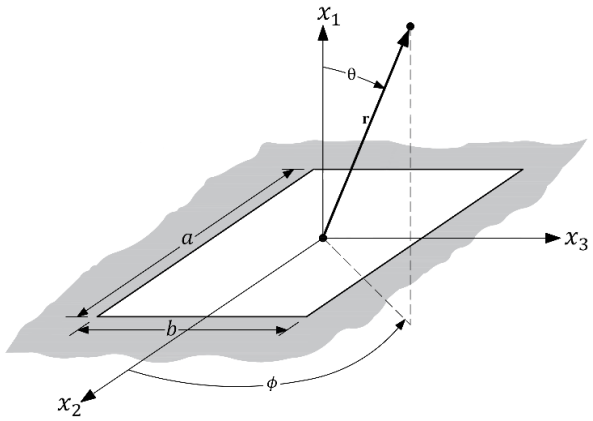

Figure 1 A rectangular aperture mounted on an infinite ground plane

The radiation fields under TE_{10} dominant mode excitation is given in [1] as

$$E_\theta(\theta,\phi)=-\frac{\pi}{2}C\sin\phi\frac{\cos X}{(X)^2-(\pi/2)^2}\frac{\sin Y}{Y} \tag{3}$$

$$E_\phi(\theta,\phi)=-\frac{\pi}{2}C\cos\theta\cos\phi\frac{\cos X}{(X)^2-(\pi/2)^2}\frac{\sin Y}{Y} \tag{4}$$

with $C=iabkE_0/(2\pi)$, $X=(ka/2)\sin\theta\cos\phi$, $Y=(kb/2)\sin\theta\sin\phi$ and $E_0=\text{const.}$ By equating (3), (4) to (1), (2), the directional currents for RAA are obtained as

$$I_m(\theta,\phi)=\pi abE_0\frac{\cos X}{X^2-(\pi/2)^2}\frac{\sin Y}{Y},\quad I_e(\theta,\phi)=0 \tag{5}$$

and typical radiation fields are depicted in Fig.2. If $\phi=0^o$, the directional currents are obtained by applying L'Hôpital's rule as

$$I_m(\theta,\phi=0^o)=\pi abE_0\frac{\cos X}{X^2-(\pi/2)^2}\cos Y,\quad I_e(\theta,\phi=0^o)=0$$

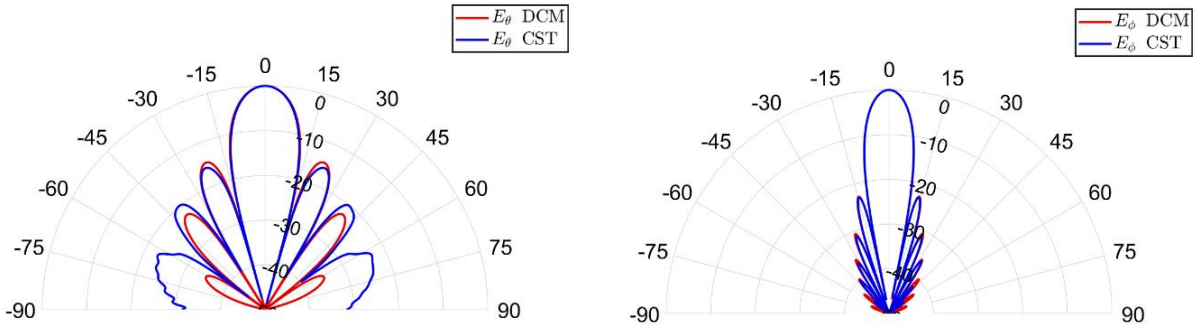

Figure 2 Free space radiation fields of the RAA by DCM and CST™ for $f=10[\text{GHz}]$, $a=2b=7.52\lambda$.

2.2. Circular Aperture Mounted on an Infinite Ground Plane

The radiation fields of circular aperture antenna (CAA) with radius a_w on an infinite ground plane as illustrated in Figure 3 under TE_{11} dominant mode excitation are given in [1] as

$$E_\theta(\theta,\phi)=C_2\sin\phi\frac{J_1(Z)}{Z} \tag{6}$$

$$E_\phi(\theta,\phi)=C_2\cos\theta\cos\phi\frac{J_1'(Z)}{1-(Z/p_{11})^2} \tag{7}$$

Here, $C_2=ika_wE_0J_1(p_{11})$, $E_0=\text{contant}$, $p_{11}=1.8412$ and $Z=ka_w\sin\theta$. $J_1(Z)$ is the first order Bessel function and $J_1'(Z)=J_0(Z)-J_1(Z)/Z$ is its first derivative with $J_0(Z)$ being the zeroth order Bessel function. By equating (6), (7) to (1), (2), the directional currents for CAA are obtained as

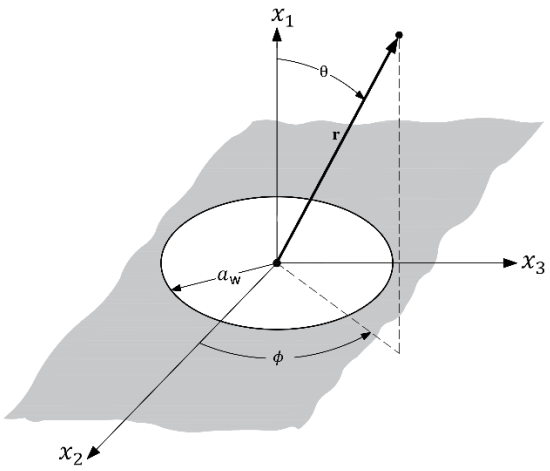

Figure 3 Circular Aperture Mounted on an Infinite Ground Plane

$$I_m(\theta,\phi) = -4\pi a_w E_0 J_1(p_{11}) \frac{1}{\sin^2\theta}\left[\frac{J_1(Z)}{Z} - \frac{J_1'(Z)}{1-(Z/p_{11})^2}\cos^2\theta\right],$$
$$I_e(\theta,\phi) = -4\pi a_w \frac{E_0}{\eta} J_1(p_{11})\cos\theta \frac{1}{\sin^2\theta}\left[\frac{J_1(Z)}{Z} - \frac{J_1'(Z)}{1-(Z/p_{11})^2}\right] \quad (8)$$

and the corresponding radiation fields are depicted in Figure 4.

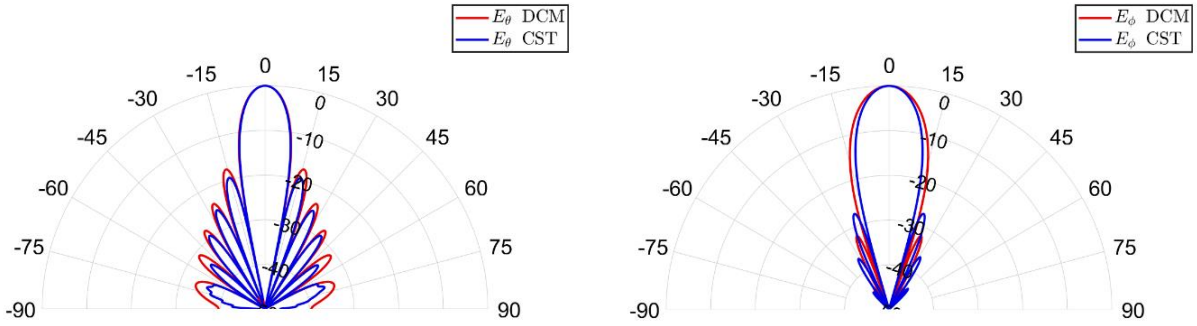

Figure 4 Free space radiation fields of the CAA by DCM and CST™ for $f = 10[\text{GHz}]$, $a_w = 3\lambda$.

2.3. Dielectric-Coated Rectangular and Circular Apertures

The aperture of the antennas may be coated with a dielectric material as illustrated in Figure 5 to protect the antennas from environmental conditions. The far-field radiation of the dielectric-coated aperture antennas are related to the uncoated ones by [1]

$$E_\theta(\theta,\phi) = f(\theta)E_\theta^0(\theta,\phi), \quad E_\phi(\theta,\phi) = g(\theta)E_\phi^0(\theta,\phi)$$

where E_θ^0 and E_ϕ^0 are the radiation fields of uncoated aperture antennas in (3), (4) and (6), (7), and

$$f(\theta)=\frac{e^{ikh\cos\theta}}{\cos\psi+iZ_h\sin\psi},\quad g(\theta)=\frac{e^{ikh\cos\theta}}{\cos\psi+iZ_e\sin\psi},$$

with

$$\psi=kh\sqrt{\varepsilon_r-\sin^2\theta},\quad Z_e=\frac{\cos\theta}{\sqrt{\varepsilon_r-\sin^2\theta}},\quad Z_h=\frac{\sqrt{\varepsilon_r-\sin^2\theta}}{\varepsilon_r\cos\theta}.$$

Here h is the thickness and ε_r is the relative permittivity of the simple dielectric layer.

The radiation fields for the dielectric-coated rectangular aperture antenna (DRAA) are given by [1]

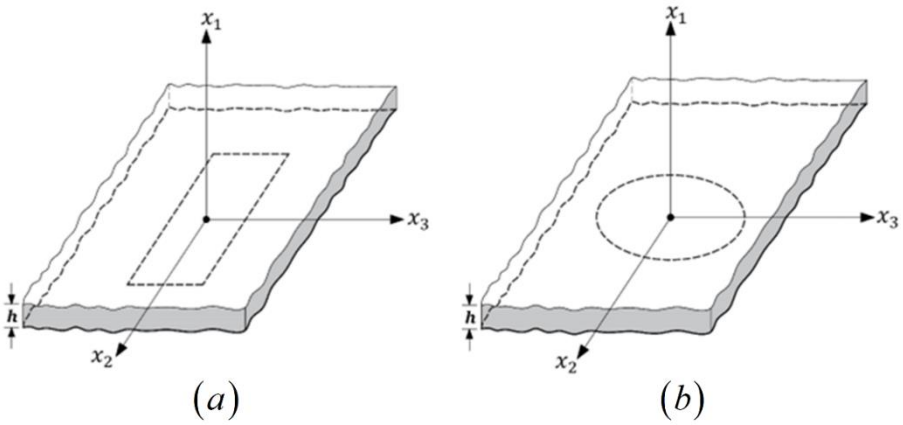

Figure 5 The Dielectric-Coated (a) Rectangular Aperture Antenna (b) Circular Aperture Antenna Mounted on an Infinite Ground Plane

$$E_\theta(\theta,\phi)=-\frac{\pi}{2}C\sin\phi\frac{\cos X}{(X)^2-(\pi/2)^2}\frac{\sin Y}{Y}f(\theta) \tag{9}$$

$$E_\phi(\theta,\phi)=-\frac{\pi}{2}C\cos\theta\cos\phi\frac{\cos X}{(X)^2-(\pi/2)^2}\frac{\sin Y}{Y}g(\theta) \tag{10}$$

and those for dielectric-coated circular aperture antenna (DCAA) are given by [1]

$$E_\theta(\theta,\phi)=C_2\sin\phi\frac{J_1(Z)}{Z}f(\theta) \tag{11}$$

$$E_\phi(\theta,\phi)=C_2\cos\theta\cos\phi\frac{J_1'(Z)}{1-(Z/p_{11})^2}g(\theta) \tag{12}$$

By equating (9), (10) to (1), (2), the directional currents for DRAA are obtained as

$$I_m(\theta,\phi) = \pi abE_0 \frac{\cos X}{(X)^2-(\pi/2)^2}\frac{\sin Y}{Y}\frac{1}{\sin^2\theta}\left[f(\theta)-g(\theta)\cos^2(\theta)\right],$$
$$I_e(\theta,\phi) = \pi ab\frac{E_0}{\eta}\frac{\cos X}{(X)^2-(\pi/2)^2}\frac{\sin Y}{Y}\cos\theta\frac{1}{\sin^2\theta}\left[f(\theta)-g(\theta)\right] \quad (13)$$

For $\phi = 0^o$, L'Hôpital's rule reveals

$$I_m(\theta,\phi) = \pi abE_0 \frac{\cos X}{(X)^2-(\pi/2)^2}\cos Y\frac{1}{\sin^2\theta}\left[f(\theta)-g(\theta)\cos^2(\theta)\right],$$
$$I_e(\theta,\phi) = \pi ab\frac{E_0}{\eta}\frac{\cos X}{(X)^2-(\pi/2)^2}\cos Y\cos\theta\frac{1}{\sin^2\theta}\left[f(\theta)-g(\theta)\right]$$

The directional currents for DCAA are obtained by equating (11), (12) to (1), (2) as

$$I_m(\theta,\phi) = -4\pi a_w E_0 J_1(p_{11})\frac{1}{\sin^2\theta}\left[\frac{J_1(Z)}{Z}f(\theta)-\frac{J_1'(Z)}{1-(Z/p_{11})^2}g(\theta)\cos^2\theta\right],$$
$$I_e(\theta,\phi) = -4\pi a_w\frac{E_0}{\eta}J_1(p_{11})\cos\theta\frac{1}{\sin^2\theta}\left[\frac{J_1(Z)}{Z}f(\theta)-\frac{J_1'(Z)}{1-(Z/p_{11})^2}g(\theta)\right] \quad (14)$$

and the corresponding radiation fields for (13) and (14) are depicted in Figure 6 and 7, respectively for $\varepsilon_r = 4.3$ and $h = 0.125\lambda$.

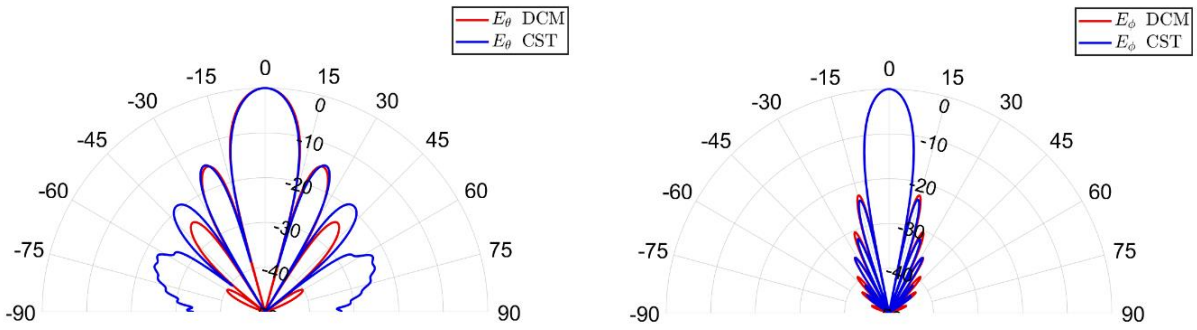

Figure 6 Free space radiation fields of the DRAA by DCM and CST™ for $f = 10[\text{GHz}]$, $a = 2b = 7.52\lambda$

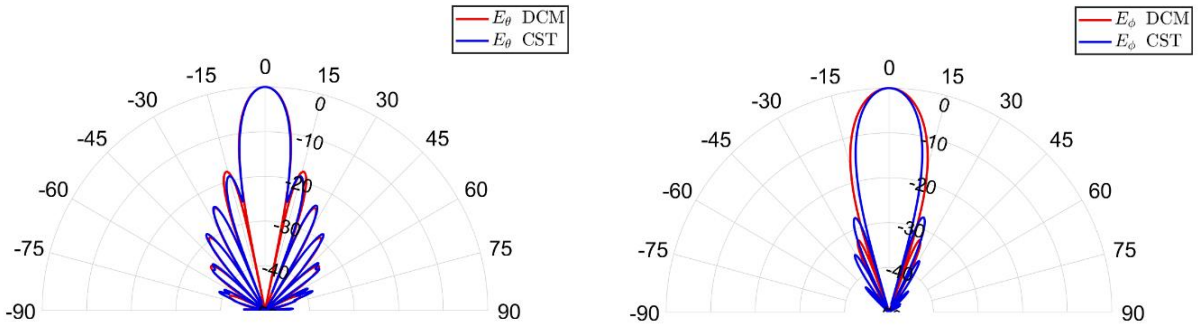

Figure 7 Free space radiation fields of the DCAA by DCM and CST™ for $f = 10[\mathrm{GHz}]$, $a_w = 3\lambda$.

2.4. E-Plane Sectoral Horn

An E-plane sectoral horn antenna (EPSHA) is produced when the rectangular end of the waveguide is flared only in the direction of the E-field [1],[2], as illustrated in Figure 8.

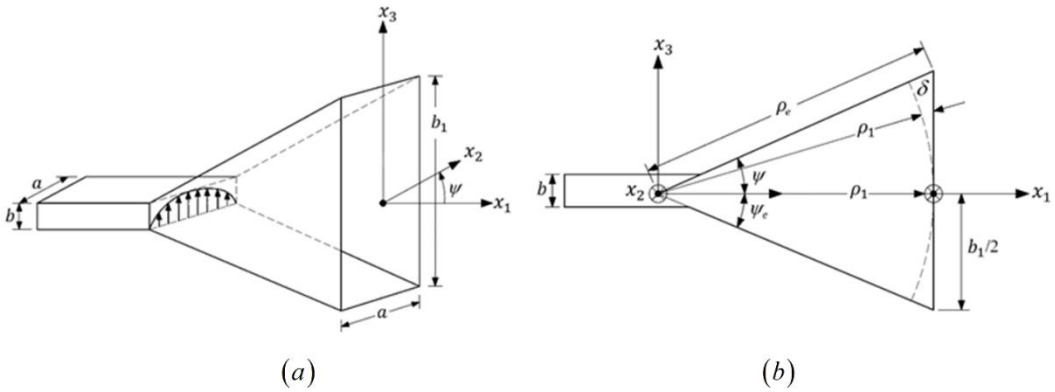

Figure 8 (a) 3-D View of the E-Plane Sectoral Horn (b) E-Plane View of the E-Plane Sectoral Horn

This is reproduced from [1] and [3], with aperture dimensions of a and b_1 $(b_1 > a)$. Due to sectoral horns having broad patterns in the plane of narrower edge, they have rarely used as radiators. A line feed for a cylindrical reflector is a potential application [1]. The far-field components radiated by the horn can be obtained from [1] under the dominant TE_{10} dominant mode excitation

$$E_\theta(\theta,\phi) = i\frac{a\sqrt{\pi k\rho_1}E_1}{8}\times\left\{e^{-i\left(k_y^2\rho_1/2k\right)}\sin\phi\left(1+\cos\theta\right)\left[\frac{\cos\left(k_x a/2\right)}{\left(k_x a/2\right)^2-\left(\pi/2\right)^2}\right]F\left(t_1,t_2\right)\right\} \qquad (15)$$

$$E_\phi(\theta,\phi) = i\frac{a\sqrt{\pi k\rho_1}E_1}{8}\times\left\{e^{-i\left(k_y^2\rho_1/2k\right)}\cos\phi\left(1+\cos\theta\right)\left[\frac{\cos\left(k_x a/2\right)}{\left(k_x a/2\right)^2-\left(\pi/2\right)^2}\right]F\left(t_1,t_2\right)\right\} \qquad (16)$$

where E_1 is constant and

$$k_x = k\sin\theta\cos\phi,\ k_y = k\sin\theta\sin\phi,$$

$$t_1 = \frac{1}{\sqrt{\pi k\rho_1}}\left(-\frac{kb_1}{2} - k_y\rho_1\right),\ t_2 = \frac{1}{\sqrt{\pi k\rho_1}}\left(\frac{kb_1}{2} - k_y\rho_1\right),$$

$F(t_1,t_2) = \left[C(t_2) - C(t_1)\right] - i\left[S(t_2) - S(t_1)\right]$ with sine and cosine Fresnel integrals defined by

$$S(x) = \int_0^x \sin\left(\frac{\pi}{2}t^2\right)dt, \qquad C(x) = \int_0^x \cos\left(\frac{\pi}{2}t^2\right)dt.$$

Then, by equating (15), (16) to (1), (2), the directional currents for E-plane sectoral horn are obtained as

$$I_m(\theta,\phi) = -\frac{1}{2}\pi a E_1\sqrt{\frac{\pi\rho_1}{k}}e^{-i\left(k_y^2\rho_1/2k\right)}\frac{\cos\left(k_x a/2\right)}{\left(k_x a/2\right)^2 - \left(\pi/2\right)^2}F(t_1,t_2),\quad I_e(\theta,\phi) = -\frac{1}{\eta}I_m(\theta,\phi) \qquad (17)$$

and the corresponding radiation fields are depicted in Figure 9.

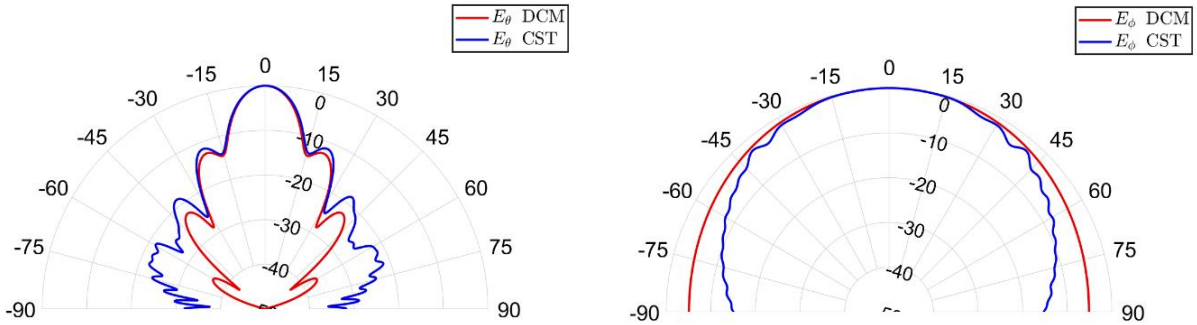

Figure 9 Free space radiation fields of the EPSHA by DCM and CST™ for $f = 10[\text{GHz}]$, $a = 2b = 0.762\lambda$, $b_1 = 3.76\lambda$, $\rho_1 = 10.5\lambda$

2.5. H-Plane Sectoral Horn

When the end of rectangular waveguide is flared only in the direction of the H-field, it forms an H-plane sectoral horn antenna (HPSHA) [1,2], as illustrated in Figure 10 with aperture dimensions of a_1 and b $(a_1 > b)$. The electric far-field components can then be expressed under the dominant TE_{10} mode as [1]

$$E_\theta(\theta,\phi) = -iE_2 \frac{b}{8}\sqrt{\frac{k\rho_2}{\pi}} \times \left\{ \sin\phi(1+\cos\theta)\frac{\sin Y}{Y}\left(e^{if_1}F(t_1',t_2') + e^{if_2}F(t_1'',t_2'')\right)\right\} \quad (18)$$

$$E_\phi(\theta,\phi) = -iE_2 \frac{b}{8}\sqrt{\frac{k\rho_2}{\pi}} \times \left\{ \cos\phi(1+\cos\theta)\frac{\sin Y}{Y}\left(e^{if_1}F(t_1',t_2') + e^{if_2}F(t_1'',t_2'')\right)\right\} \quad (19)$$

where E_2 is constant, ρ_2 is the radial distance from the apex to a point on the aperture in the H-plane, and

$$t_1' = \sqrt{\frac{1}{\pi k\rho_2}}\left(-\frac{ka_1}{2} - k_x'\rho_2\right),\ t_2' = \sqrt{\frac{1}{\pi k\rho_2}}\left(\frac{ka_1}{2} - k_x'\rho_2\right),\ k_x' = k\sin\theta\cos\phi + \frac{\pi}{a_1}$$

$$t_1'' = \sqrt{\frac{1}{\pi k\rho_2}}\left(-\frac{ka_1}{2} - k_x''\rho_2\right),\ t_2'' = \sqrt{\frac{1}{\pi k\rho_2}}\left(\frac{ka_1}{2} - k_x''\rho_2\right),\ k_x'' = k\sin\theta\cos\phi - \frac{\pi}{a_1}$$

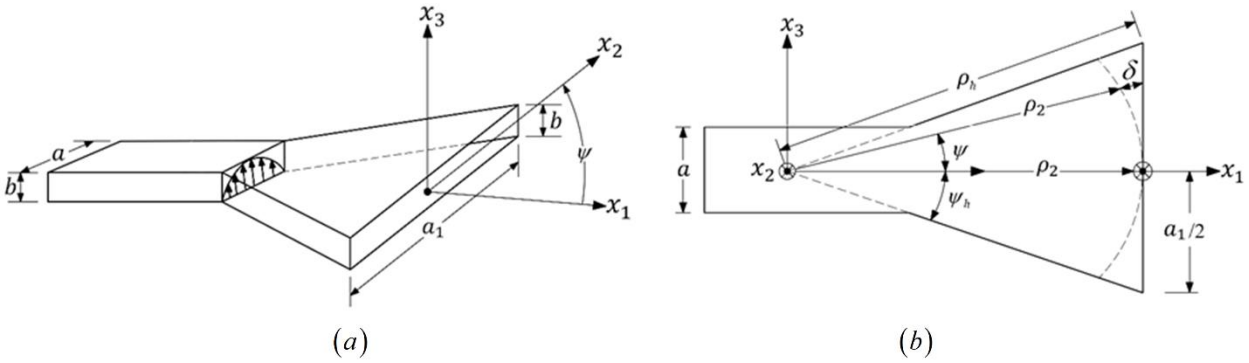

Figure 10 (a) 3-D View of the H-plane Sectoral Horn (b) H-plane View of the H-plane Sectoral Horn

$$F(t_1',t_2') = \left[C(t_2') - C(t_1')\right] - i\left[S(t_2') - S(t_1')\right],\ F(t_1'',t_2'') = \left[C(t_2'') - C(t_1'')\right] - i\left[S(t_2'') - S(t_1'')\right]$$

$$f_1 = \frac{k_x'^2\rho_2}{2k},\ f_2 = \frac{k_x''^2\rho_2}{2k}, Y = \frac{kb}{2}\sin\theta\sin\phi$$

The equivalent directional currents are given by equating (18), (19) to (1), (2) as

$$I_m(\theta,\phi) = \frac{1}{2}bE_2\sqrt{\frac{\pi\rho_2}{k}}\frac{\sin Y}{Y}\left[e^{if_1}F(t_1',t_2') + e^{if_2}F(t_1'',t_2'')\right],\quad I_e(\theta,\phi) = -\frac{1}{\eta}I_m(\theta,\phi) \quad (20)$$

For $\phi = 0^o$, L'Hôpital's rule reveals

$$I_m(\theta,\phi=0^o) = \frac{1}{2}bE_2\sqrt{\frac{\pi\rho_2}{k}}\cos Y\left[e^{if_1}F(t_1',t_2') + e^{if_2}F(t_1'',t_2'')\right]\Big|_{\phi=0^o},\ I_e(\theta,\phi=0^o) = -\frac{1}{\eta}I_m(\theta,\phi=0^o)$$

and the corresponding radiation fields are depicted in Figure 11.

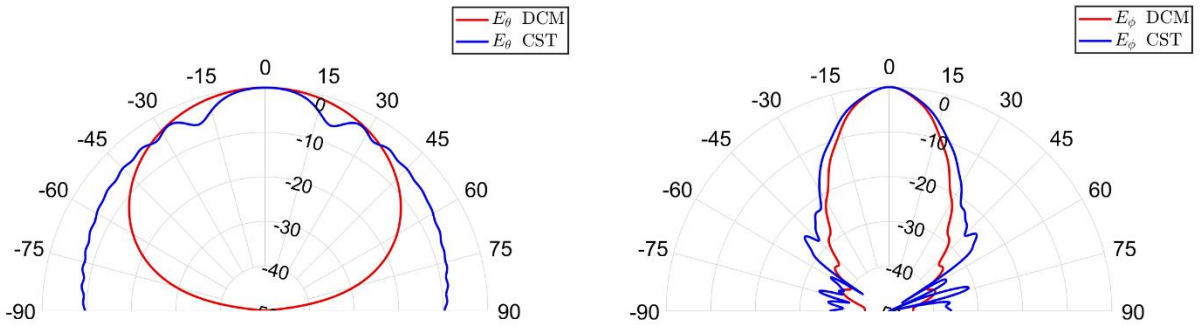

Figure 11 Free space radiation fields of the HPSHA by DCM and CST™ for $f = 10[\text{GHz}]$, $a = 2b = 0.762\lambda$, $a_1 = 7.52\lambda$, $\rho_2 = 10.5\lambda$

3. Radiation Fields of Aperture and Horn Antennas over Sea Surface

We consider the scenario in Figure 12, where the central point of the antenna under test (AUT) is situated at a height d over the sea surface. The upper half space is air with wave number $k = \omega\sqrt{\mu_0\varepsilon_0}$ and the antenna is excited in the dominant mode. This is the same scenario as in [3]-[5] in which pyramidal, conical and corrugated conical horn antennas are investigated, respectively. The constitutive parameters of lower half-space are denoted by $(\varepsilon = 80\varepsilon_0, \mu_0, \sigma = 4\,[\text{S/m}])$ and the wavenumber is given by $k_1 = Nk$, where $N^2 = \varepsilon_r(1 + i\tau)$, $\varepsilon_r = \varepsilon/\varepsilon_0$, $\tau = \sigma/\omega\varepsilon$ and $|N| = 8.96$ for the given constitutive parameters.

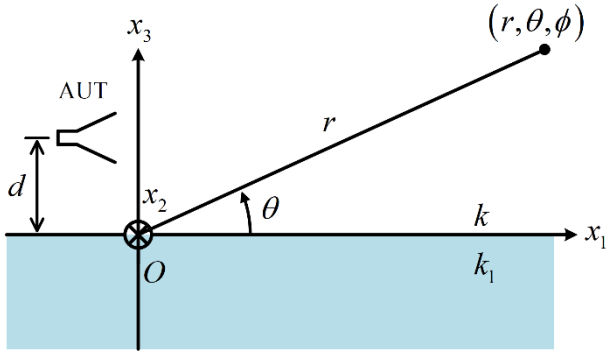

Figure 12 Antenna Under Test Radiating Over a Simple Lossy Dielectric Half-Space

The far-field radiation fields of AUT over sea surface (see [3], [4]), which use Norton's solutions under HCA $N \geq 3$ are given as follows:

E-plane radiation pattern: $\theta \in [0, \pi/2]$, $\phi = \pi/2$

$$E_\theta(r,\theta,\phi) = \frac{ik}{4\pi}\cos^2\theta\left[\eta I_e \cos\theta - I_m\right]\cdot\left[1 + R_v e^{i2kd\sin\theta} + (1-R_v)F(w)e^{i2kd\sin\theta}\right] \quad (21)$$

H-plane radiation pattern: $\theta \in [0, \pi/2]$, $\phi = 0, \pi$

$$E_\phi(r,\theta,\phi) = \frac{ik}{2\pi}\left[\eta I_e + \cos\theta I_m\right]\cos\phi F\left(\frac{ikr}{2}N^{-2}\left(1-N^{-2}\right)\right) \quad (22)$$

Here, $R_v = \dfrac{\sin\theta - \Delta_0}{\sin\theta + \Delta_0}$ is reflection coefficient with $\Delta_0 = N^{-1}\sqrt{1-N^{-2}\cos^2\theta}$ being normalized surface impedance of the sea water; and $F(w) = 1 + i\sqrt{\pi w}\,e^{-w}\,\mathrm{erfc}\left(-i\sqrt{w}\right)$ is Norton attenuation function with $w = \dfrac{ikr}{2\cos^2\theta}\left(\sin^2\theta + \Delta_0\right)^2$ being numerical distance.

The observation distance is chosen as $r = 5\,[\mathrm{km}]$. This already satisfies the far-field approximation. The distance d is chosen to set the lowest point of each antenna just above the sea surface.

The radiation fields of all antennas over sea surface are obtained by inserting the directional currents of each of the above antennas into (23) and (24). The results are depicted in Figures 13-18 with comparison to the CST™ simulations.

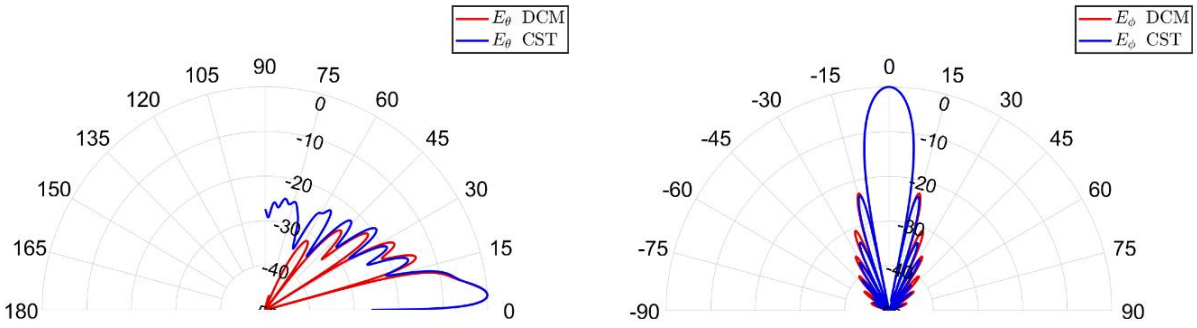

Figure 13 Radiation fields of the RAA over sea surface by DCM and CST™ for $f = 10[\mathrm{GHz}]$, $a = 2b = 7.52\lambda$.

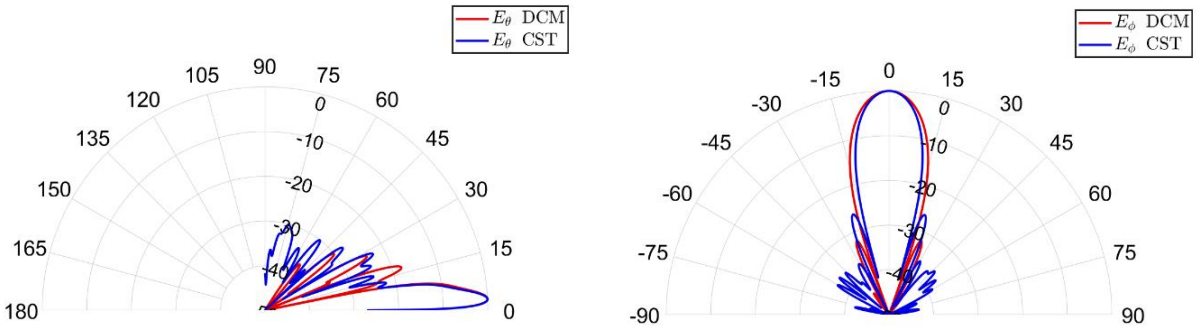

Figure 14 Radiation fields of the CAA over sea surface by DCM and CST™ for $f = 10[\mathrm{GHz}]$, $a_w = 3\lambda$.

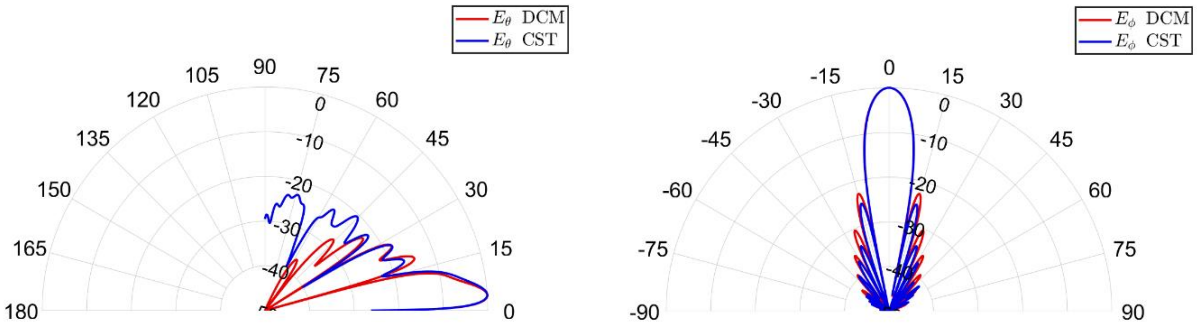

Figure 15 Radiation fields of the DRAA over ground by DCM and CST™ for $f = 10[\mathrm{GHz}]$, $a = 2b = 7.52\lambda$.

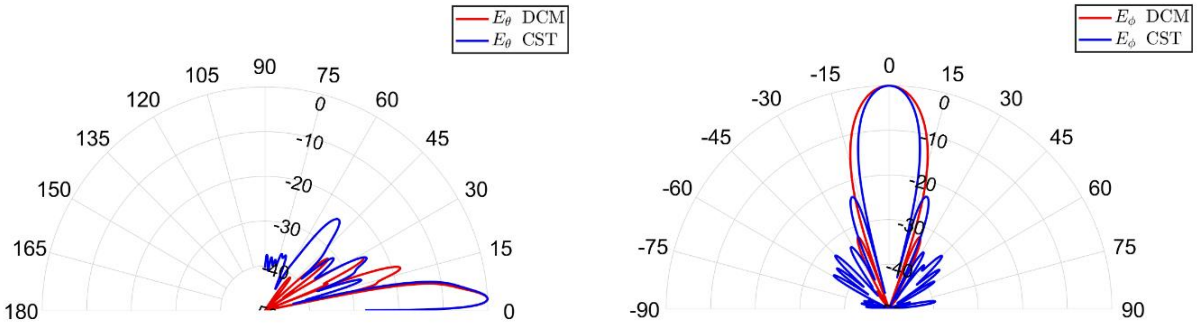

Figure 16 Radiation fields of the DCAA over sea surface by DCM and CST™ for $f = 10[\mathrm{GHz}]$, $a_w = 3\lambda$

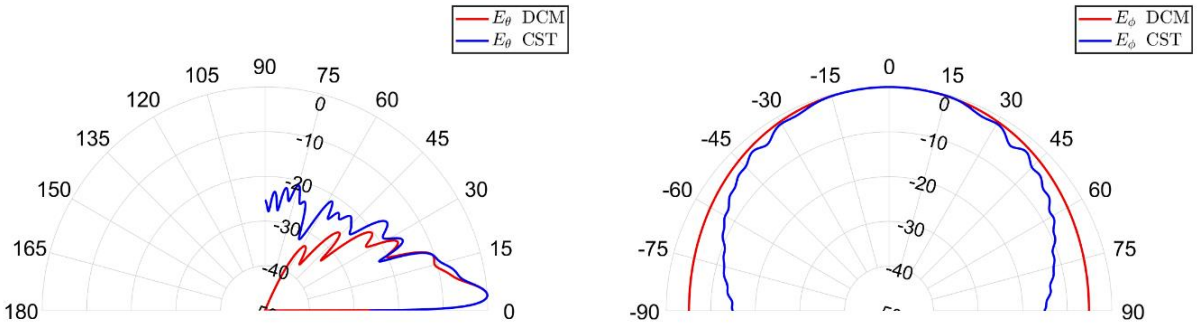

Figure 17 Radiation fields of the EPSHA over sea surface by DCM and CST™ for $f = 10[\text{GHz}]$, $a = 0.762\lambda$, $b = 0.339\lambda$ $b_1 = 3.76\lambda$, $\rho_1 = 10.5\lambda$

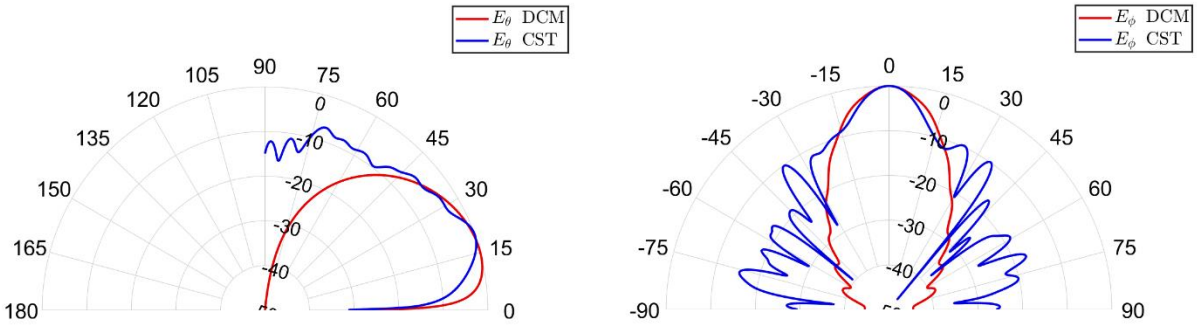

Figure 18 Radiation fields of the HPSHA over sea surface by DCM and CST™ for $f = 10[\text{GHz}]$, $a = 0.762\lambda$, $b = 0.339\lambda$, $a_1 = 7.52\lambda$, $\rho_2 = 10.5\lambda$

4. Results

Considering the radiation fields given through Figures 13–18, we observe that the elevation patterns of all antennas are tilted upward by the sea surface in both DCM and CST™ simulations in free space. Both simulations are in good agreements in the main lobes of the elevation patterns. However, in the side lobes of the antennas, DCM and CST™ results show some discrepancies. This can be attributed to the diffraction effects from the edges of antennas. These effects are involved in full wave CST™ simulations while they are disregarded in DCM. On the other hand, no significant difference in azimuth radiation patterns of antennas for DCM and CST™ simulations are observed, as expected.

DCM has a slightly less accurate performance than CST™ for the side lobes of the antennas. However, its analytically explicit results provide the advantage of computing the radiation fields over a lossy ground quite rapidly (in a few seconds). On the other

hand, CST™ requires tens of minutes for the same tasks. Such an advantage provides DCM as a powerful tool in investigating such scenarios.

5. Conclusion

In the present study we implemented DCM to the rectangular aperture antenna, circular aperture antenna, dielectric loaded rectangular and circular antennas, and E- and H-plane sectoral horn antennas. In Section 2 we calculated the directional currents for the antennas under investigation and computed the azimuth and elevation radiation patterns, then checked the validity of the calculated directional currents by the commercial electromagnetic simulator CST™. In Section 3 we applied the directional currents on the far field radiation fields of VED and HMD antennas located over sea surface to achieve the analytical far field azimuth and elevation radiation fields of the antennas interested in. Here, CST™ simulations are performed again to check the parametric accuracy of the analytical fields provided by DCM.

Based on the observations of the relative performances in Figures 13-18, certain aperture and horn antennas are planned to be manufactured and tested experimentally at Yildiz Technical University Radar Research Laboratory (YTU-RADAL). The theoretical investigations will also continue by applying DCM to other aperture-like antennas over a lossy ground.

Acknowledgement

This work was supported by Research Fund of the Yildiz Technical University. Project Number: FBA-2021-4310

References

[1] Balanis, C. A. (2016). Antenna theory: analysis and design. 4th ed. John Wiley & sons.

[2] Volakis, J. L. (2007). Antenna engineering handbook. McGraw-Hill Education.

[3] Polat, B., & Daşbaşı, R. (2020). Hertzian Dipoles Supporting Directional Currents. In 2020 IEEE Ukrainian Microwave Week (UkrMW), 494-500.

[4] Polat, B., & Daşbaşı, R. (2021). Analysis of conical horn antenna radiation over ground by directional currents method. In 2021 20th International Conference on Microwave Techniques (COMITE), 1-6.

[5] Mohammed Musa, D. S., Daşbaşı, R. & Polat, B., (2021). Radiation Fields of Corrugated Horn Antenna over Lossy Dielectric Half-Space, 5th International 19 May Innovative Scientific Approaches Congress, Samsun, Turkey, 198-210.

[6] Norton, K. A. (1937). The physical reality of space and surface waves in the radiation field of radio antennas. Proceedings of the Institute of Radio Engineers, 25(9), 1192-1202.

[7] Mclean, Z. S. M. & Wu, Z. (1993). Radiowave propagation over ground. Chapman & Hall.